Journal of Thermal Analysis and Calorimetry (2019) 138:2937–2944
https://doi.org/10.1007/s10973-019-08567-0

Thermal processing and thermal analysis of AlSi12–SiC hybrid composites sintered

Ioan Milosan[1] · Bela Varga[1] · Tibor Bedo[1] · Mihai Alin Pop[1] · Marianne Balat-Pichelin[2] · Dana Luca-Motoc[3] · Maria Stoicanescu[1]

Received: 3 December 2018 / Accepted: 8 July 2019 / Published online: 18 July 2019

Abstract
Metal powders are used in industry for a diversity of products and applications. Metal matrix composites are materials developed through advanced methods with increased characteristics that surpass those of conventional materials. In recent years, the aluminum alloy matrix composites (AlSiX/graphite, AlSiMg/SiC, Al/SiC) are considered better substitute materials for steel components because of their higher strength-to-mass ratio which results in significant mass savings, these materials being successfully used in the construction of automotive components such as brakes and clutches. The paper presents a study concerning the specificities of the sintering technology using solar energy of an AlSi12–SiC hybrid composite, made by powder metallurgy performed at PROMES-CNRS at Font-Romeu-Odeillo-France (MSSFs facility furnaces). Based on the collected data, conclusions could be drawn on the heating mode and the effect of the concentrated power of the parabola on the sintering curves recorded by thermal analysis. The qualification of the sintered samples is performed by structural, DIL and DSC analyses.

Keywords MMCs · AlSi12–SiC hybrid composites · Solar energy · Sintering · DIL · DSC

Introduction

The various technologies used to obtain composite materials aim to combine use properties that cannot be achieved by common metallurgical technologies (melting + casting). As it is known, Al–Si alloys with eutectic and hypereutectic compositions have remarkable use properties (low friction and thermal expansion coefficients and good corrosion resistance due to the formation of the compact Al_2O_3 film on the surface of the products) as well as advantageous melting and casting technological properties and good cuttability. The improvement of wear resistance follows technologies that introduce solid reinforcing particles in the base metallic mass without reducing the technological properties [1–6].

In recent years, the aluminum alloy matrix composites are considered better substitute materials for steel components because of their higher strength-to-mass ratio that results in significant mass savings.

Recent researches on Al or Al alloys composites study different variations of the combination with SiC and graphite, such as Al–Si/graphite composites [4, 7], Al–Si/CNTs/SiC composites [1], Al–Si/SiC composites [8] and graphite/Al composites [6].

The making of the composites by mixing the components in powdered state and the compaction–reinforcements thereof by pressing and subsequent sintering has some advantages compared to the classical technology of introducing the reinforcement phase into the liquid alloy followed by casting.

The specificity of this paper is that the pressed specimens are sintered using solar energy, which, as it is known, is a source of non-polluting energy, available in unlimited

✉ Ioan Milosan
milosan@unitbv.ro

[1] Department of Materials Science, Faculty of Materials Science and Engineering, Transilvania University of Brasov, 1 Universităţii Str., 500068 Brasov, Romania

[2] PROMES-CNRS Laboratory, 7 rue du Four Solaire, 66120 Font Romeu Odeillo, France

[3] Department of Vehicles and Transport, Faculty of Mechanical Engineering, Transilvania University of Brasov, 29 Eroilor Bld., 500036 Brasov, Romania

quantities [9–12]. The specificity of solar energy is also given by the fact that the way it is used manages to concentrate great power on a small surface. It should be noted that its drawback is the impossibility of planning the necessary energy, as well as the difficulty in regulating the absorbed energy according to the needs.

The paper analyzes the stability of the thermal conditions during sintering and its effect on the quality of the sintered products. The sintering regimes were characterized by simple thermal analysis, and the sintered products were characterized by structural analysis using an optical microscope, by DSC/DIL analyses, preferred methods of analysis in specialized scientific research [13–24].

Experimental research

Material selection and sample manufacturing

The composite specimens were obtained by mixing AlSi12 powder, 99% (metal basis) code 88322, average grain size of 325 mesh (44 μm) with silicon carbide (SiC) powder, superfine, 600 grit, with an average grain size of 137 μm and density of 3.16 g cm^{-3}. The powders were purchased from Alfa Aesar (USA).

The components (AlSi12 powder and silicon carbide powder) were mixed in a Mini Lab Powder Mixer YLK Brand, at the speed of 50 rpm, within a controlled atmosphere for 60 s.

Four types of material mixtures were obtained, in the following variants:

- *variant 1* samples made only of AlSi12 powder (0% SiC added);
- *variant 2* samples made of AlSi12 powder + 2% SiC added;
- *variant 3* samples made of AlSi12 powder + 5% SiC added;
- *variant 4* samples made of AlSi12 powder + 10% SiC added.

The specimens were coded using the figure expressing the concentration of the reinforcement phase (SiC) in the composite. The mixture was dosed in the pressing die volumetrically. The pills were pressed using a UTT-type hydraulic press, at a pressing force of 500 and 750 MPa, for 15 s. The samples were obtained in the form of cylindrical pills, 16 mm in diameter and 6 ± 1 mm in height. Several pills for each of the four compositions mentioned above were made.

Composite sample conditioning

Solar energy sintering

Composite specimens were sintered by aid solar energy, a vertical axis medium-sized solar furnace of 1 kW power at CNRS-PROMES laboratory, Font-Romeu in France with the manual adjustment of the shutter (Fig. 1). The incident solar radiation was characterized by the DNI (direct normal irradiance) ranged between 850 and 980 W m^{-2}, and the heating rate varied between 0.5 and 1.5 C s^{-1}.

Laboratory furnace sintering

Another sintering route of the herein composite samples deployed an in situ laboratory furnace (Research Institute of the Transilvania University of Brasov—PRO-DD) designed for heat treatments, based on electrical resistances.

Composite characterization

The structural analysis was performed by aid of an optical microscope (Nikon-Omnimet-Buehler) with different magnifications (e.g., ×25, ×1000).

The specific differential scanning calorimetry (DSC) tests were conducted with the "DSC 200 F3 Maia" thermal analysis equipment. Within these measurements, the solid-state phase transformations at different temperatures (between RT—room temperature—and 600 °C) were carefully studied. The applied DSC testing parameters were:

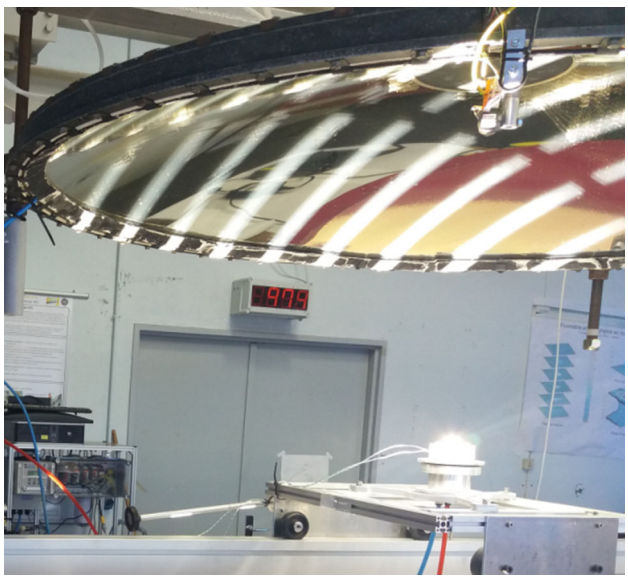

Fig. 1 Sintering of AlSi12–SiC composites using the medium-sized solar furnace at the CNRS-PROMES laboratory, Font-Romeu (France)

maximum testing temperature + 600 °C; minimum testing temperature RT; heating/cooling rate 10 K min^{-1}; nitrogen gas as protection atmosphere with a constant debit of 20 mL min^{-1}.

NETZCH Proteus—Thermal Analysis—version 5.2.1 software was used for processing the DSC experiment. The dilatation peaks were established on both the cooling curve and the heating curve, together with the transformation enthalpy.

Specimens' expansivity was monitored by aid of a push rod dilatometer DIL L75/230 (Linseis, D), in controlled atmosphere, within 25–550 °C temperature range deploying 2.5 K min^{-1} heating rate in the dynamic step. The experimental runs comply the ASTM E228:2011 standard procedures. Specimens' dimensions were set as 25 mm × 5 mm in length and width, respectively. Accompanying software enabled outcomes retrieval, such as the coefficient of linear thermal expansion (CLTE or α) and transformation phases along with corresponding temperatures.

Sintering

Sintering with solar energy In the preliminary sintering experimental determinations, there were experimented different ways of heating the pills: direct heating; heating in a refractory enclosure, with cover made of a refractory material; and heating in a refractory enclosure with a 3-mm-thick refractory steel plate cover fulfilling the role of "heating element." As the light spot was focused on this cover, the heating of the samples in the refractory chamber was done in the same conditions as in a classical sintering furnace, with electrical resistors. Considering the fact that the third heating option (Fig. 2) gave the best results in terms of control of the thermal regime and uniformity of the temperature on the specimen height, the studied specimens were sintered using this variant.

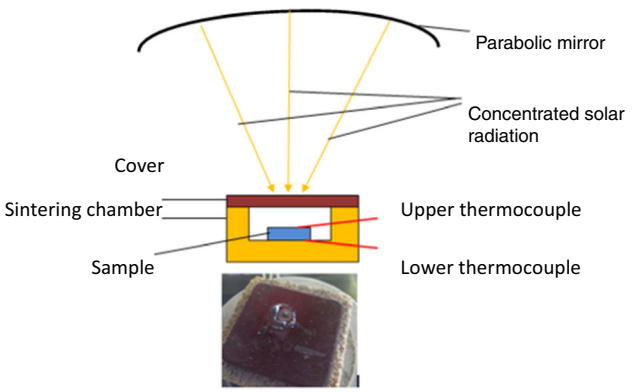

Fig. 2 Technological variant adopted for the sintering of the specimens in the solar furnace: top—schematic representation, bottom—refractory enclosure coated with a refractory steel plate

The temperature in the sintering chamber was recorded using 2K-type thermocouples, located above and below the samples (Fig. 2). The data were recorded using a "Data Logger EL-GFX-DTC, Dual Channel K type Thermocouple with Graphic Screen."

The optimum sintering range, considering the composition of the base material (AlSi12), was considered to be the 550–430 °C temperature range (the lower limit of the sintering temperature is 0.75 of the melting temperature of the alloy).

During the sintering using solar energy (see Fig. 2), there were recorded a number of parameters: the maximum available power of the installation during the sintering operations, the heating/holding/cooling times, as well as the temperature variation on the upper and lower surfaces of the specimens, as shown in Table 1.

In Fig. 3 is shown the temperature profile retrieved for sample 5-1 sintered by aid of solar energy.

Due to inconsistencies in the solar energy flux during exposure session covering different time length (a.m. to p.m.), minor adjustments should be made to the optical components in order to compensate the temperature difference on upper and bottom surfaces. This difference due to the lower power provided by the solar furnace is provided in Table 1 and represented in Fig. 4.

Sintering with laboratory furnace (PRO-DD)

Sintering using classical technology In parallel, there were sintered a number of pills (specimens) in the Research Institute of the Transilvania University of Brasov (PRO-DD) using the classical technology in a laboratory furnace with a chamber, designed for heat treatments, heated with electrical resistances, according to the diagram in Fig. 5. These specimens were coded by adding the "c" (classical) index to the number expressing the concentration of SiC particles in the composite.

As it can be seen, based on the data shown in Table 1 and Fig. 5, during the sintering of the specimens in the solar furnace, the heating times are much lower than in the case of sintering using the classical technology and, therefore, the holding time was increased in this case.

Results and discussion

Structural analysis

The structural analyses reveal a uniform distribution of reinforcing particles (SiC) within the AlSi12 matrix, as shown in Fig. 6.

During the sintering operations, the dimensions of the globular silicon separations increased, and, at the end, the

Table 1 The parameters of the sintering process in the solar furnace—example for the AlSi12–5% SiC specimens

Sample code[a]	Pressing force/MPa	Maximum DNI during sintering/W m^{-2}	Average temperature on the surface/°C		Times/min	
			Upper	lower	heating	holding
5-1	750	851	545	500	8	10
5-1	500	862	538	505	10.35	10
5-2	750	875	510	420	6	15
5-2	500	943	510	500	5	15
5-3	750	901	560	430	9.30	15
5-3	500	921	550	500	9	15

[a]Remark: In the sample code, the figure following the sample number is the number of parallel sintering's for the specimens with the same SiC content. The pressing force will be indicated by filling in the sample code with its value

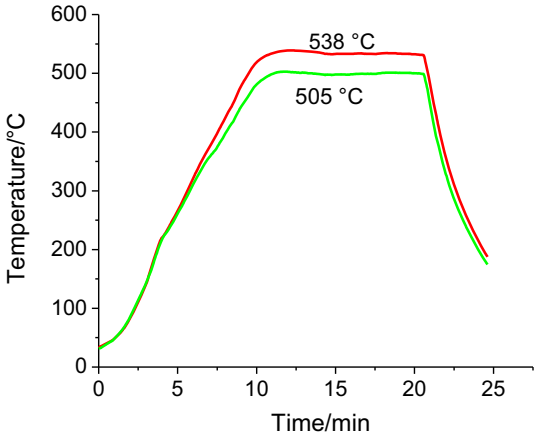

Fig. 3 Temperature profile during the sintering specific to the sample 5-1/500 (5% SiC, pressed at 500 MPa); red line—thermocouple placed on the sample surface; green line—thermocouple placed at the base of the sample. (Color figure online)

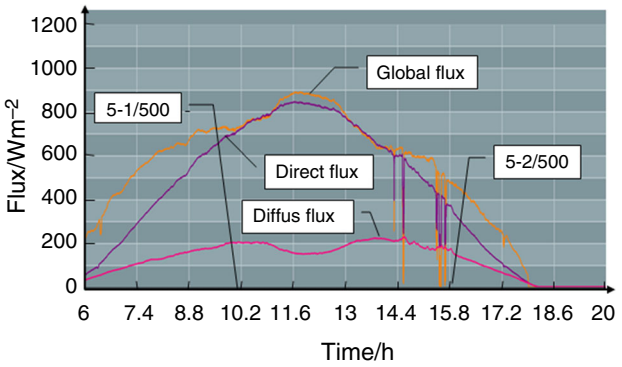

Fig. 4 Variation of the solar flux (DNI) on 8 September 2017, between 6 am and 8 pm, with the indication of the sintered specimens

structure of the base metallic mass became hypoeutectic, although in terms of composition the alloy is eutectic.

This structural "anomaly" is due to the technology used to obtain the powder of the alloy with eutectic composition (AlSi12). Due to the high cooling speeds, the eutectic point

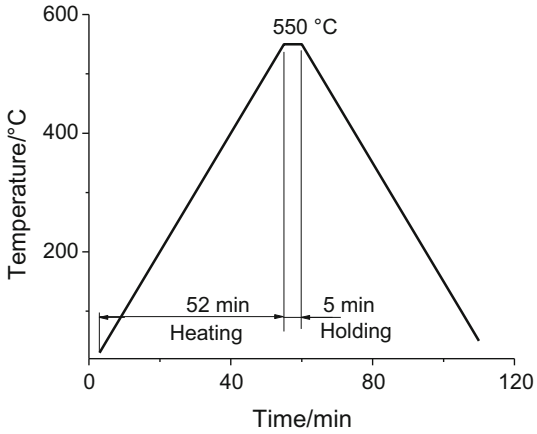

Fig. 5 Diagram of sintering using the classical technology

moves to the right, and thus, the eutectic composition of the alloy becomes structurally hypoeutectic. As can be seen in the pressed sample (see Fig. 7a), the dimensions of the silicon separations are less than one micron.

There should be noted that the increase in the dimensions of the globular silicon separations during the sintering operation is caused by the silicon exiting the solid solution, supersaturated in this element, which was formed during the processing of the aluminum powder, as shown in Fig. 7b, c.

The dimensions of the silicon separations in the two sintering technologies are comparable, of approximately 2 μm; larger separations, of 5 μm, are present in samples sintered using the classical technology.

The structures presented in Fig. 8 highlight some phenomena adversely affecting the properties of the composites. Thus, during the pressing, cracking (the breaking of the reinforcement particles (SiC) becomes possible, as shown in Fig. 8a, or the matrix can have a non-homogeneous structure because of the instability of the temperature profile during the sintering in the solar furnace (Fig. 8b).

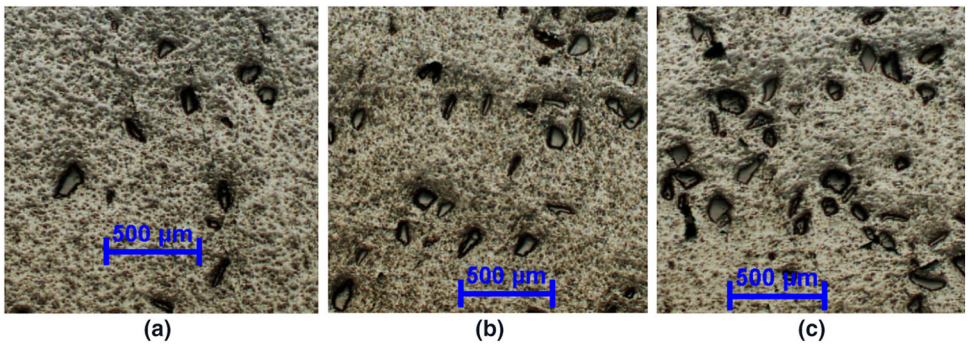

Fig. 6 Distribution of SiC particles in the matrix for samples with: **a** 2% SiC; **b** 5% SiC; **c** 10% SiC, ×25

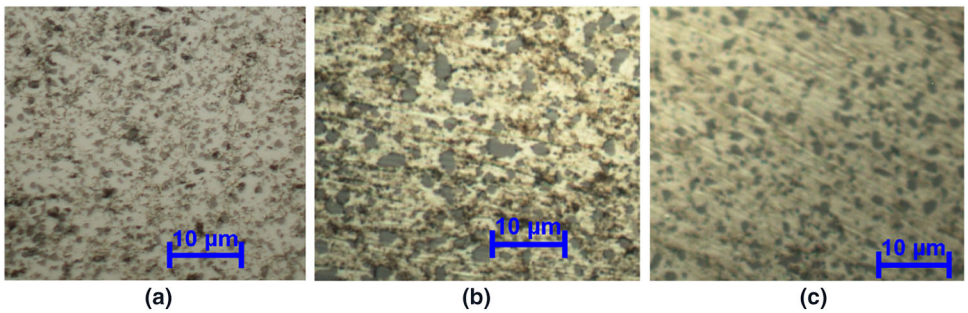

Fig. 7 Structure of the base metallic mass for the composite with 5% SiC after pressing and sintering: **a** after pressing; **b** sintering using the classical technology (sample 5c); **c** in the solar furnace (sample 5-2/500, Table 1), ×1000

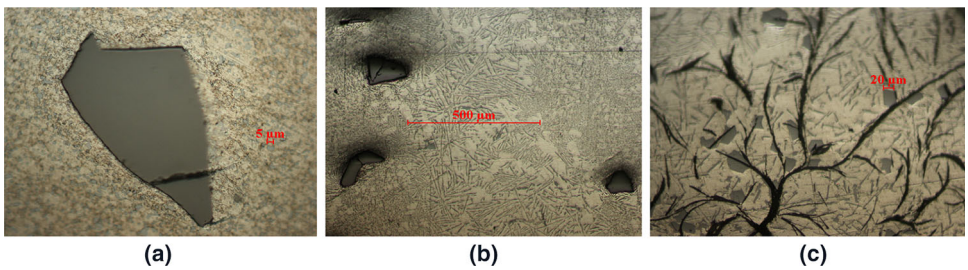

Fig. 8 Defects in processed composites: **a** rupture of SiC particles (sample 5c) ×500; **b** non-homogeneous structure (sample 2c), ×200; **c** the non-homogeneous and oxidized structure of the melted specimen (sample 10c) ×200

The non-homogeneous structure also manifests itself by the formation of areas of significant width (500 µm) with eutectic structure with acicular silicon, as shown in Fig. 8b. The defect can be related to the instability of the solar flux.

At the same time, there is shown the structure of the base metallic mass for a sample melted during the sintering in the solar furnace, which, after solidification, shows coarse primary silicon separation (20 µm) in a base metallic mass consisting of eutectic, with acicular silicon, and Al_2O_3 films at the alloy granules limits, Fig. 8c.

DSC and DIL analyses

In order to analyze the phenomena occurring during the sintering, the pressed (non-sintered) samples made of basic alloy (AlSi12) and of the composites with 2, 5 and 10% SiC were subjected to DSC and DIL analyses according to the parameters in the sintering diagram using the classical technology, shown in Fig. 3.

The results of the DSC analysis for the AlSi12 powder and the 5% SiC composite are shown in the diagrams in Fig. 9. Figure 9a shows the DSC (heating + cooling) curves for the massive AlSi12 alloy, with the equilibrium structure consisting of eutectic silicon and a solid equilibrium solution with less than 1.5% silicon. Therefore, the DSC curves, both during heating and cooling, reveal no phase changes within room temperature range—the eutectic temperature, which would correspond to a solid-state transformation.

The DSC curves shown for the massive alloy and the AlSi12 powder highlight that the technology used to obtain the AlSi12 powder significantly influences the behavior of the alloy during heating (sintering). At the same time, the DSC curves plotted for powder and composite highlight that the presence of solid SiC particles in the composite has no major effect on the decomposition of the solid solution supersaturated in silicon. The process by which silicon exits the supersaturated solid solution occurs at approximately the same temperature, the first peak in Fig. 9b. The fact that the reinforcement particles influence the behavior (growth) of the silicon after its exit from the supersaturated solid solution, also suggested by the shape of the DSC

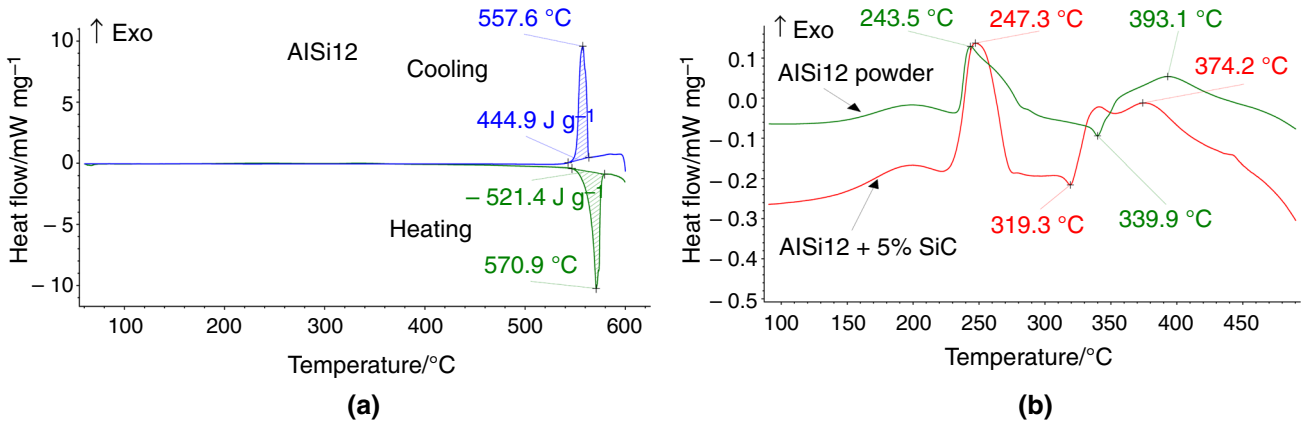

Fig. 9 DSC curve for: **a** the massive AlSi12 alloy with the equilibrium structure **b** the AlSi12 powder (variant 1) and the 5% SiC composite

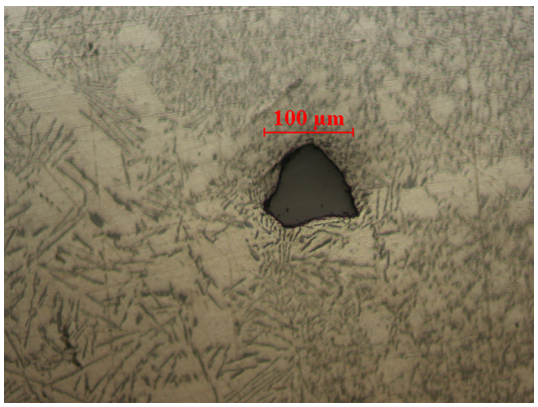

Fig. 10 Silicon separations around the SiC particle, sample with 2% SiC (2-c-I), ×200

curves, is also confirmed by the shape/dimensions of the eutectic silicon around the SiC particles, shown in Fig. 10.

Figure 11 shows the curves presenting the variation of the physical expansion coefficient according to the temperature, when sintering the specimens with 0, 2, 5 and 10% SiC.

The purpose of these analyses is to study the structural changes occurring during the sintering operations and, afterward, during use. From this point of view, the peaks on these curves, which correspond to changes in the expansion of samples caused by the phase transformations and not by the thermal expansion, are of interest. The expansion curves could only be recorded for the classical sintering, in the dilatometer itself (Fig. 11a); these determinations were denoted by "I," according to the sample code. Figure 11b shows the results obtained during a second heating, denoted by "II," according to the sample code.

The values (coordinates) corresponding to the main characteristic points (peaks) in Fig. 11a, denoted by **[a]**, **[b]**, **[c]** and **[d]**, are summarized in Table 2.

In Fig. 11a, the peaks marked with **[a], [c], [d]** correspond to the maximum intensity of the transformation processes during the heating operation (sintering), the first two are produced with increasing volume and the last with a decrease in volume. The peak marked with **[b]** represents the end of the silicon exit process from the supersaturated solid solution.

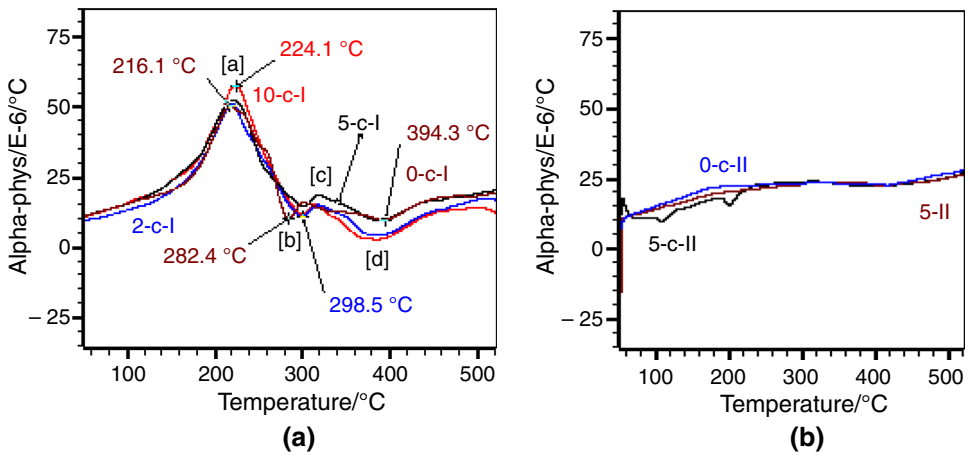

Fig. 11 Variation of the physical expansion coefficient according to the temperature: **a** in the sintering of specimens containing 0, 2, 5 and 10% SiC; **b** in the second heating

Table 2 The coordinates of the characteristic points [a], [b], [c] and [d] in Fig. 11

Sample code	Peak/a		Peak/b		Peak/c		Peak/d	
	t/°C	$\alpha \times 10^{-6}$/°C^{-1}	t/°C	$\alpha \times 10^{-6}$/°C^{-1}	t/°C	$\alpha \times 10^{-6}$/°C^{-1}	t/°C	$\alpha \times 10^{-6}$/°C^{-1}
0-c-I	216.1	51.2	282.4	11.3	300	16.7	394.3	10.5
2-c-I	218.6	51.8	298.5	11.9	317.4	15.9	386.1	5.1
5-c-I	218.6	53.4	302.4	15.5	318.5	19.4	390.3	10.5
10-c-I	224.1	58.4	303.3	12.5	315.9	16.3	385.1	3.5

The dilatometric analysis highlighted no significant differences between the behavior of the base alloy (0% SiC) and the composites with 2, 5, 10% SiC. In all composites, the decomposition of the solid solution (peak **'a'**) occurs at a temperature by about 2.5–8 °C higher than the one at which this process occurs in the base alloy, 216.1 °C.

Following the expansion caused by the exit of silicon from the supersaturated solid solution, the variation curve of the physical expansion coefficient has a minimum value **[b].**

In the case of the alloy (with no reinforcement particles), this minimum value is of 282.4 °C. The presence of solid SiC particles causes the shifting of this minimum value toward higher temperatures by 6–11 °C. There should be noted that this difference is highlighted both by the DSC curves in Fig. 9a and the micrograph in Fig. 10.

For the third characteristic point, the peak **[d]**, the solid particles of SiC cause this point to move to the right by about 16 °C. During the second heating, Fig. 11b, the variation curves of the expansion coefficient almost overlap, and thus, they behave similarly.

The overlapping of these curves also suggests that the equilibrium state of the base metallic material is achieved by sintering. This remark is of particular importance in terms of behavior of these materials during use. There should be noted that, during the sintering of the analyzed composites, the physical expansion coefficient varies between 5×10^{-6} and 68×10^{-6} C^{-1}, which can adversely affect the integrity of the specimens.

Conclusions

The analysis of the results presented in this paper yields the following conclusions:

1. The powder used in the experimental determinations, following the sintering process, has a hypoeutectic structure, although the alloy is chemically eutectic;
2. The presence of solid SiC particles have no significantly influence upon the mechanism of silicon exiting (during sintering) the supersaturated solid solution, but it influences its growth, coagulation thereof.
3. It should be emphasized that the structure of specimens sintered in the solar furnace has much smaller (2 μm) silicon separations compared to the sintering via the classical technology that has 5-μm silicon separations as well.
4. The equilibrium state of the alloy is structurally achieved during sintering.
5. Achieving proper results for the sintering of AlSi12 + SiC particles by using solar energy requires the use of the automatic adjustment of the solar energy transmitted to the sintering unit.

Acknowledgements The financial support offered by the Access to Research Infrastructures activity in the 7th Framework Programme of the EU (SFERA 2 Grant Agreement No. 312643) is gratefully acknowledged, as well as the use of the facilities and the researchers/technology experts at the PROMES-CNRS laboratory. We hereby acknowledge the structural funds project PRO-DD (POS-CCE, O.2.2.1., ID 123, SMIS 2637, Contract No. 11/2009) for providing the infrastructure used in this paper.

References

1. Carvalho O, Buciumeanu M, Madeira S, Soares D, Silva FS, Miranda G. Mechanisms governing the mechanical behaviour of an AlSi–CNTs–SiCp hybrid composite. Compos B. 2016;90:443–9.
2. Narciso J, Molina JM, Rodriguez A, Rodriguez-Reinoso F, Louis E. Effects of infiltration pressure on mechanical properties of Ale12Si/graphite composites for piston engines. Compos B. 2016;91:441–7.
3. Alpas AT, Zhang J. Effect of SiC particulate reinforcement on the dry sliding wear of aluminium–silicon alloys (A356). Wear. 1993;155:81–104.
4. Rajaram G, Kumaran S, Satyam S. Effect of strain rate on tensile and compression behaviour of Al–Si/graphite composite. Mater Sci Eng A. 2011;528:6271–8.
5. Goto H, Uchijo K. Wear mechanism of Al–Si Alloy impregnated graphite composites under dry sliding. Wear. 2005;259:613–9.
6. Xue C, Bai H, Tao PF, Wang JW, Jiang N, Wang SL. Thermal conductivity and mechanical properties of flake graphite/Al composite with a SiC nano-layer on graphite surface. Mater Des. 2016;108:250–8.

7. Shanmughasundaram P, Subramanian R. Study of parametric optimization of burr formation in step drilling of eutectic Al–Si alloy–Gr composites. J Mater Res Technol. 2014;3(2):150–7.
8. Madeira S, Carvalho O, Carneir VH, Soares D, Silva FS, Miranda G. Damping capacity and dynamic modulus of hot pressed AlSi composites reinforced with different SiC particle sized. Compos B. 2016;90:399–405.
9. Flamant G, Ferriere A, Laplaze D, Monty C. Solar processing of materials: opportunities and new frontiers. Sol Energy. 1999;66(2):117–32.
10. Rodriguez GP, Lopez V, Vazquez AJ, De Damborenea JJ, Kirkpatrick A, Worek W. Solar Engineering. New York: ASME; 1993. p. 325–30.
11. Flamant G, Balat-Pichelin M, Elaboration and testing of materials using concentrated solar energy. Encyclopedia of Life Support Systems. Eolss Publisher Co. Ltd./UNESCO United Kingdon; 2010. p. 363–89.
12. Sarver T, Al-Qaraghuli A, Kazmerski Lawrence L. A comprehensive review of the impact of dust on the use of solar energy: history, investigations, results, literature, and mitigation approaches. Renew Sustain Energy Rev. 2013;22:698–733.
13. Balek V, Zeleňák V, Mitsuhashi T, Bakardjieva S, Šubrt J, Haneda H. Emanation thermal analysis of SiC based materials. J Therm Anal Calorim. 2002;67(1):83–9.
14. Balek V, Beneš M, Šubrt J. Use of emanation thermal analysis in the microstructure diagnostics of alumina coatings. Ceram-Silik. 2008;52(2):85–9.
15. Pérez-Maqueda LA, Balek V, Poyato J, Pérez-Rodriquez JL, Šubrt J, Bountsewa IM, Beckman IN, Málek Z. Study of natural and ion exchanged vermiculite by emanation thermal analysis, TG, DTA and XED. J Therm Anal Calorim. 2003;71:715–26.
16. Gaune-Escard M. Calorimetric Methods. Molten Salt Technics, vol. 4. New York: Plenum Press; 1991. p. 152–92.
17. Ghosh KS. Calorimetric studies of 2024 Al–Cu–Mg and 2014 Al–Cu–Mg-Si alloys of various tempers. J Therm Anal Calorim. 2019;136:447–59.
18. Snopiński P, Król M, Tański T, Krupińska B. Effect of cooling rate on microstructural development in alloy ALMG9. J Therm Anal Calorim. 2018;133:379–90.
19. Król M, Tański T, Snopiński P, Tomiczek B. Structure and properties of aluminium-magnesium casting alloys after heat treatment. J Therm Anal Calorim. 2017;127:299–308.
20. Labisz K, Konieczny J, Jurczyk S, Tański T, Krupiński M. Thermo-derivate analysis of Al–Si–Cu alloy used for surface treatment. J Therm Anal Calorim. 2017;129:895–903.
21. Brodarac ZZ, Grgurić TH, Burja J. Thermodynamic stability of AlSi11 alloy microconstituents. J Therm Anal Calorim. 2017;127:431–8.
22. Mostafapoor S, Malekan M, Emamy M. Thermal analysis study on the grain refinement of Al–15Zn–2.5Mg–2.5Cu alloy. J Therm Anal Calorim. 2017;127:1941–52.
23. Farahany S, Ourdjini A, Idris MH. The usage of computer-aided cooling curve thermal analysis to optimise eutectic refiner and modifier in Al–Si alloys. J Therm Anal Calorim. 2012;109:105–11.
24. Daoudi MI, Triki A, Redjaimia A. DSC study of the linetic parameters of the metastable phases formation during non-isothermal annealing of an Al–Si–Mg alloy. J Therm Anal Calorim. 2011;104:627–33.